CHEMISTRY OF MATERIALS

Subscriber access provided by La Trobe University Library

Article

Self-Assembly of CTAB and Lamellar Zeolite Precursor for the Preparation of Hierarchical MWW Zeolite

Le Xu, Xinyi Ji, Shenhui Li, Zhengyang Zhou, Xin Du, Junliang Sun, Feng Deng, Shunai Che, and Peng Wu

Chem. Mater., **Just Accepted Manuscript** • DOI: 10.1021/acs.chemmater.6b02155 • Publication Date (Web): 06 Jun 2016

Downloaded from http://pubs.acs.org on June 11, 2016

Just Accepted

"Just Accepted" manuscripts have been peer-reviewed and accepted for publication. They are posted online prior to technical editing, formatting for publication and author proofing. The American Chemical Society provides "Just Accepted" as a free service to the research community to expedite the dissemination of scientific material as soon as possible after acceptance. "Just Accepted" manuscripts appear in full in PDF format accompanied by an HTML abstract. "Just Accepted" manuscripts have been fully peer reviewed, but should not be considered the official version of record. They are accessible to all readers and citable by the Digital Object Identifier (DOI®). "Just Accepted" is an optional service offered to authors. Therefore, the "Just Accepted" Web site may not include all articles that will be published in the journal. After a manuscript is technically edited and formatted, it will be removed from the "Just Accepted" Web site and published as an ASAP article. Note that technical editing may introduce minor changes to the manuscript text and/or graphics which could affect content, and all legal disclaimers and ethical guidelines that apply to the journal pertain. ACS cannot be held responsible for errors or consequences arising from the use of information contained in these "Just Accepted" manuscripts.

ACS Publications

Chemistry of Materials is published by the American Chemical Society. 1155 Sixteenth Street N.W., Washington, DC 20036

Published by American Chemical Society. Copyright © American Chemical Society. However, no copyright claim is made to original U.S. Government works, or works produced by employees of any Commonwealth realm Crown government in the course of their duties.

Self-Assembly of CTAB and Lamellar Zeolite Precursor for the Preparation of Hierarchical MWW Zeolite

Le Xu[†§], Xinyi Ji[†], Shenhui Li[‡], Zhengyang Zhou[§], Xin Du[§], Junliang Sun[§], Feng Deng[‡], Shunai Che[#], and Peng Wu*[†]

[†] Shanghai Key Laboratory of Green Chemistry and Chemical Processes, School of Chemistry and Molecular Engineering, East China Normal University, Shanghai 200062, PR China.

[‡] State Key Laboratory of Magnetic Resonance and Atomic and Molecular Physics, National Center for Magnetic Resonance in Wuhan, Wuhan Institute of Physics and Mathematics, Chinese Academy of Sciences, Wuhan 430071, PR China.

[#] State Key Laboratory of Metal Matrix Composites, School of Chemistry and Chemical Engineering, Shanghai Jiao Tong University, Shanghai 200240, PR China.

[§] College of Chemistry and Molecular Engineering, Peking University, Beijing 100871, PR China.

ABSTRACT: Construction of hierarchical zeolite catalysts from lamellar zeolite precursor is challenging and promising for industrial catalysis. Although numerous efforts have been dedicated to control the organization of zeolite nanosheets by post-synthetic approaches or employing complex surfactants in hydrothermal synthesis, there is still no successful case that the hierarchical lamellar zeolite is hydrothermally synthesized by the self-assembly of the commercially available simple surfactant cetyltrimethylammonium bromide (CTAB) and inorganic zeolite precursor. In traditional syntheses, the self-assembly of simple surfactants and the growth of microporous framework are hardly compatible from both thermodynamic and kinetic viewpoints, preferring to cause phase separation. Herein, we approach for the first time the hydrothermal synthesis of a mesostructured multilamellar zeolite ECNU-7P, consisting of an alternative stacking of inorganic MWW zeolite nanosheets and organic CTAB layers with large interlayer spacing (25 Å), by a zeolite seed and CTAB-assisted dissolution-recrystallization route. Correlated 2D ^{1}H-^{29}Si solid-state NMR, X-ray, electron microscopy and rotation electron diffraction analyses provide molecular-level insights into the guest-host interactions between organic surfactant and inorganic framework during the self-assembly and structure evolution process. Moreover, the calcined Al-ECNU-7 possessing a hierarchical mesostructure proves to serve as a highly active, selective and stable solid acid catalyst for triisopropylbenzene cracking as well as acylation of anisole.

Zeolites are crystalline microporous materials, which have been widely used as heterogeneous catalysts in oil refining and petrochemicals industries.[1-3] However, the presence of sole micropores in conventional zeolites inevitably hinders their actual use in processing bulky molecules due to severe mass transfer limitation. Introducing mesoporosity into traditional zeolite crystals would reduce diffusion path lengths and maximize the structural functionalities in the limited space.[4-10] Post-synthetic approaches, such as dealumination and desilication, are useful to generate intracrystal mesopores, but they should be delicately controlled to prevent the loss of crystallinity. In comparison with post-synthetic approaches, hydrothermal synthesis of hierarchical zeolites through soft-template route adopting bulky organic molecules is more expected due to the more precise control of mesopore formation.

Layered zeolite precursor is a particularly attractive intermediate to design hierarchical material because of the diversity of zeolite layers stacking, which could derive various zeolitic materials possessing open structures.[11-15] Various post-synthetic strategies have been proposed such as the phase exfoliation of layered structures.[16-20] Although the exfoliated zeolites exhibit greatly enhanced catalytic activities in many reactions, the post-synthetic approaches, usually operated in strong basic media, are possible to cause the amorphization or dissolution of crystalline frameworks.[12,16,21-23] Thus, the direct synthesis of hierarchical layered materials with the aid of soft-templates is strongly desirable. Ryoo and coworkers succeeded in synthesizing zeolite nanosheets using several rationally-designed Gemini-type surfactants containing at least two quaternary ammonium head groups,[24-25] which exhibited dual structure-directing functionalities at different length scale, resulting in the multilamellar MFI nanosheets with unit-cell thickness.[26] Similarly, single-crystalline mesostructured zeolite nanosheets (SCZN)[27-29] and MIT-1[30] that were composed of the MFI or MWW zeolite nanosheets, respectively were also directly synthesized in the presence of precisely-designed bifunctional surfactants. Corma and coworkers presented the direct synthesis of a material containing a large proportion of MWW monolayers by combining hexamethyleneimine with a designed bifunctional surfactant containing 1,4-diazabicyclo[2.2.2]octane (DABOCO) groups.[31] However, it was demonstrated that the syntheses of these kind of hierarchical lamellar zeolite much relied on the directing function of complex supramolecular surfactants in micro- and mesoscale. Therefore, the multi-ammonium cations should be carefully designed to have the dual function of directing the growth of crystalline zeolite framework and balancing the self-assembly of zeolite layers. On the contrary, to the best of our knowledge, no successful

example that the hierarchical lamellar zeolite is prepared by the self-assembly of the commercially available monoquaternary ammonium surfactant and inorganic zeolite layers has been realized.

In traditional syntheses, the simple surfactant CTAB was highly expected to cooperate with the organic structure-directing agent (OSDA) in hydrothermal synthesis, leading to the direct crystallization of hierarchical zeolites. However, these two types of organic templates with different properties hardly act in a synergistic manner, but in fact, they usually compete to direct independently the formation of mesopores and micropores, leading to phase separation. Generally, the self-assembly of surfactant molecules and the growth of microporous crystalline framework are incompatible with each other from both thermodynamic and kinetic viewpoints. Consequently, it is difficult to achieve highly-ordered zeolite phases and mesostructures simultaneously, even when a complex multiammonium surfactant is adopted. Thus, it is regarded as a well-known challenge in the field of hierarchical zeolite to discover controllable systems in which the simple surfactant and inorganic crystalline zeolite phase can self-assemble cooperatively to generate micro- and mesoporous materials with simplicity and potential industrial viability.

In this contribution, we approached for the first time the hydrothermal preparation of a mesostructured multilamellar MWW zeolite ECNU-7P by controllable self-assembling of simple surfactant CTAB and lamellar zeolite precursors through a zeolite seed and CTAB-assisted dissolution-recrystallization route. The small quaternary ammonium hydroxide, 1,3-*bis*(cyclohexyl)imidazolium hydroxide, was used as the small OSDA to direct the crystallization of MWW sheets, whereas the bulky CTAB surfactants pillared the layers thus constructed. The combination of the characterizations, such as 2D ^{1}H-^{29}Si solid-state NMR, X-ray, electron microscopy and rotation electron diffraction (RED) analyses, provided molecular-level insights into the interactions between CTAB molecules with respect to crystalline zeolite layers. The cationic hydrophilic head group of CTAB had a strong interaction with the inorganic zeolite layer and was embedded in the hemi-cavities on the MWW layer surface, while its hydrophobic long-chain alkyl group (C_{16}) supported the neighboring MWW nanosheets, resulting in alternative self-assembly of inorganic zeolite layers and organic CTAB layers in the multilamellar zeolite ECNU-7P. With the assistance of MWW zeolite seed, the Al-containing ECNU-7P could be synthesized in a wide range of Si/Al ratios (15 ~ ∞). The calcined Al-ECNU-7 with hierarchical structure exhibited excellent activity, selectivity and stability in the catalytic reactions involving bulky molecules.

EXPERIMENTAL SECTION

Synthesis of organic structure-directing agent (OSDA). 1,3-*bis*(cyclohexyl)imidazolium hydroxide (IM^+OH^-) was employed as the OSDA for the crystallization of MWW zeolite. The synthesis procedure and characterization of the organic compound are represented in Supporting Information, which are the same as those reported previously.[32]

Synthesis of multilamellar precursor ECNU-7P and hierarchical zeolite ECNU-7. Multilamellar precursor ECNU-7P was synthesized using dual organic templates, those were, IM^+OH^- as the OSDA for crystallizing microporous MWW topology and commercially available CTAB surfactant as the organic pillars to generate secondary pore architecture in mesoscale. The mixture of fumed silica (AEROSIL 200) and the calcined ITQ-1 silicate (its detailed synthesis procedure was shown in Supporting Information) was used as the starting silica source, in which the molar percentage of fumed silica was varied as 0, 25, 50, 75 and 100 %. In a typical synthesis, the silica source (fumed silica and ITQ-1 seed) was added to an aqueous solution of IM^+OH^- under stirring at room temperature for 1 h, resulting in the gel A with a molar composition of 1.0 SiO_2 : 0.5 IM^+OH^- : 25 H_2O. The gel A was transferred into an autoclave and reacted at 443 K for 1 h under rotation, and then cooled to room temperature quickly to obtain the gel B. Subsequently, the aluminum source $NaAlO_2$ (44.3 % Al_2O_3, 37.5 % Na_2O) and CTAB surfactant were introduced into the gel B, giving a mixture with final molar composition of 1.0 SiO_2 : 0.5 IM^+OH^- : 25 H_2O : (0 ~ $^1/_{30}$) Al_2O_3 : 1.0 CTAB. The resulting gel was sealed in an autoclave and further treated at 423 K under rotation condition. After crystallization for a period of time, the product ECNU-7P (Si/Al = 15 ~ ∞) was obtained after filtration and dried at 353 K. The OSDAs and surfactants were removed by calcination in air at 873 K for 6 h, giving rise to a hierarchical zeolite ECNU-7. Besides, the pillaring of the multilamellar Al-ECNU-7P was performed according to the method reported previously.[33] For control experiment, the conventional MCM-22 aluminosilicate was synthesized according to that reported in the literature,[34] while the MCM-56 analogue was post-synthesized from the as-made MCM-22 precursor by a mild acid treatment.[35]

RESULTS AND DISCUSSION

Synthesis and characterization of multilamellar zeolite ECNU-7P. The syntheses of the swelling-type multilamellar MWW zeolite were tried under various hydrothermal conditions using CTAB and IM^+OH^- as soft templates. IM^+OH^- has been demonstrated to possess the ability for directing the MWW topology.[32] The syntheses were carried out using the pre-prepared MWW-type silicate (well known as ITQ-1) or the mixture of ITQ-1 and amorphous silica as the starting material. A very successful result was obtained in the case of Al-ECNU-7P (Si/Al = 50) with 3D MWW ITQ-1 as the sole starting material, in which the MWW sheets were stacked in an ordered manner (Figure 1Ea).[36] Taking this as the representative, the crystallization process could be divided into two stages. At Stage I, the starting silica source (the calcined ITQ-1 silicate in this case) was mixed with the IM^+OH^- solution to give the gel A, which was hydrothermally treated at 443 K for 1 h to degrade the crystalline structure of original MWW zeolite to obtain the gel B. Then, the aluminum source together with the simple surfactant CTAB were introduced into the resulting gel B, and then the synthesis continued at 423 K in Stage II. The Stage I was the same as the early procedure that we reported in the synthesis of novel layered zeolite ECNU-5P,[32] during which the crystals of MWW silicate were dissolved significantly in the basic medium as the MWW framework greatly collapsed within 1 h, giving a solid yield of only 17.8 wt.% (Figure 1Cb). The remaining solid exhibited somewhat broadened PXRD peaks with reduced intensity, which was attributed to the residual crystalline MWW phase (Figure 1Ab and 1Bb). Thus, the dissolved silicate fragments in liquid phase as well as the remaining solid phase, both still containing or consisting of the basic building units of the MWW structure, may act as nutrient species for crystallization in the next synthesis stage.

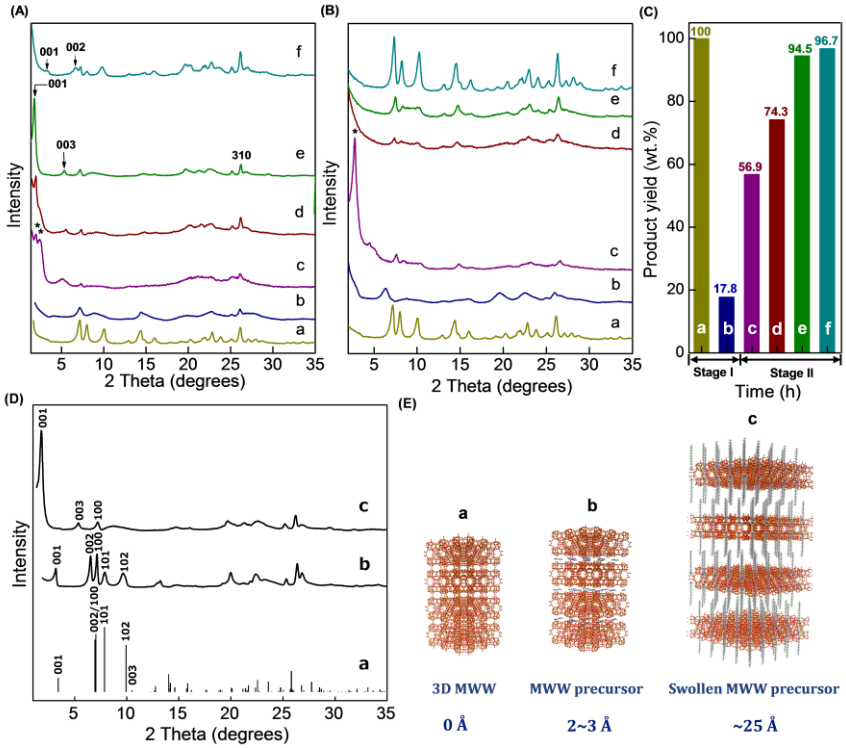

Figure 1. Powder XRD patterns of (A) as-synthesized, (B) calcined products and (C) their corresponding solid yields based on SiO_2 during the crystallization of Al-ECNU-7P (Si/Al = 50, with ITQ-1 as sole starting silica source): (a) the parent ITQ-1, (b) stage I: 443 K, 1 h, stage II: 423 K for (c) 24 h, (d) 48 h, (e) 72 h, (f) 96 h; (D) PXRD patterns and (E) structural models of (a) simulated 3D MWW structure, (b) conventional MWW layered precursor, (c) Al-ECNU-7P (in swelling form). The numbers in Figure 1E show the interlayer spacing of adjacent MWW layers.

After hydrothermal treatment at 423 K in Stage II, the dissolved silica species were recrystallized in the presence of IM^+OH^- and CTAB, which was indicated by the gradual increase of solid yields (Figure 1C). For the product obtained after hydrothermal treatment at 423 K for 24 h, two peaks newly appeared in the low-angle region of PXRD patterns (2θ = 1.9° ~ 2.5°), and the calcination shifted the peak to 2.8° and enhanced the diffraction intensity (Figure 1Ac and 1Bc). Besides, the products were mainly of sphere morphology together with a small content of platelet-like crystals (Figure 2b). These results implied that the silica fragments in gel B were presumably reassembled into a hexagonal mesoporous phase as well as lamellar phase with the assistance of CTAB molecules.

Further prolonging the time to 48 h gave rise to a lamellar phase, which showed a more intense peak at 2θ = 1.9° together with a shoulder at 2θ = 2.4° (Figure 1Ad), both of which disappeared after calcination (Figure 1Bd). The SEM images showed that the sample was packed into a lamellar phase (Figure 2c), indicating that the hexagonal mesostructure obtained previously might have been transformed to a 2D layered phase. Besides, the peaks assigned to the MWW structure in high-angle region were still not well resolved (Figure 1Ad and 1Bd), implying the crystallization of zeolite framework did not occur to a high degree.

After the treatment for 72 h, the product showed a strong and narrow PXRD peak at 2θ = 1.76° together with well-resolved ones in high-angle region, corresponding to the MWW structure (Figure 1Ae and 1Be). This indicated that the ordering of multilamellar structure increased even after a full crystallization of the MWW structure. The low-angle peak at 2θ = 1.76° can be assigned to the first-order 001 reflection corresponding to the interlayer structural correlation. Figure 1D compared in detail the PXRD patterns of conventional MWW and representative sample prepared in this study. The first-order 001 reflection observed at 2θ = 1.76° corresponded to d_{001} = 50 Å (Figure 1Dc). Considering the fact that the MWW monolayer had a thickness of 25 Å,[37] the interlayer spacing, possibly generated as a result of the surfactant molecules pillaring two adjacent MWW sheets, was calculated to be 25 Å. The absence of the 002 reflection is probably because of the "accidental extinction" when the layer thickness and interlayer spacing are comparable.[38] These phenomena have already been well observed and addressed for the multilamellar MFI zeolites.[12,38] Nevertheless, the third-order 003 reflection appeared obviously at 2θ = 5.28°, indicating the presence of an ordered layered structure in the long range. Thus, Al-ECNU-7P (Si/Al = 50) with an alternative stacking of MWW layers and organic pillars along *c* axis might be obtained after the hydrothermal synthesis reaction for 72 h in Stage II (Figure 1Ec). The resulting Al-ECNU-7P zeolite showed a uniform platelet-like morphology. Although the crystal edge for each MWW monolayers could not be determined owing to ultrathin crystal thickness, the layered stacking manner was clearly observed (Figure 2d). Besides, the calcined sample Al-ECNU-7 showed a broad PXRD peak with a low intensity in the 2θ range of 8° ~ 10.5° (Figure 1Be), which resembled those of previously reported EMM-10P,[39] MCM-56,[35,40] SSZ-70[41] and ECNU-5.[32] The MWW layers in Al-ECNU-7P were assumed to be twisted or disordered in plane, lacking the discrete interlayer reflections especially for the 101 and 102 planes.

When the reaction mixture was further heated in autoclave for 96 h in Stage II, a conventional MWW layered

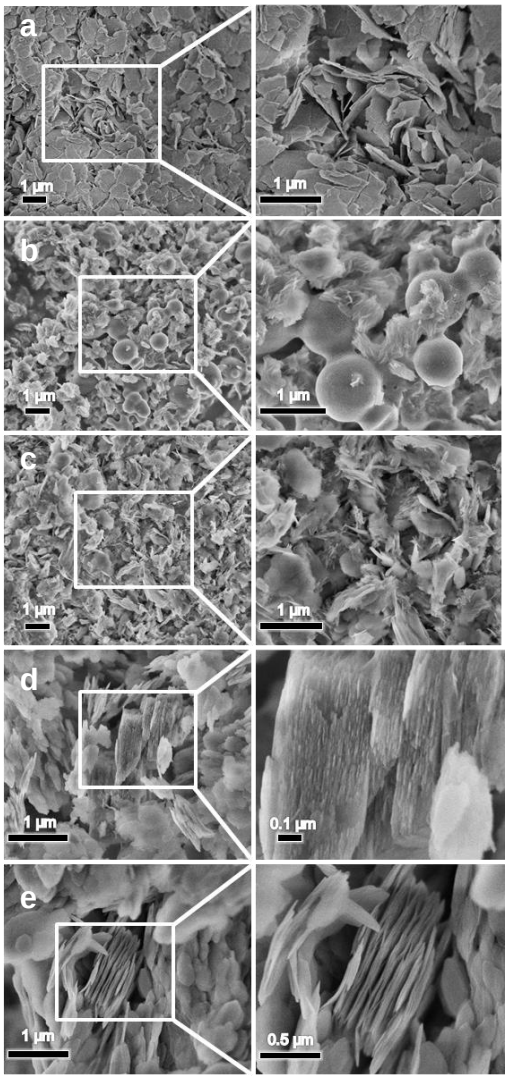

Figure 2. SEM images of the samples obtained during the synthesis process of Al-ECNU-7P (Si/Al = 50). (a) the parent MWW silicate; crystallized in Stage II for (b) 24 h; (c) 48 h; (d) 72 h; (e) 96 h.

precursor was obtained, which showed the characteristic 001 and 002 reflections at 2θ = 3.3° and 6.6°, respectively (Figure 1Af), corresponding to a narrowed interlayer spacing of 2 Å (Figure 1Eb). Its calcined form turned into the normal 3D MWW structure showing extremely intensive and well resolved reflections (Figure 1Bf and 1Ea), meanwhile still exhibiting a platelet-like crystal morphology (Figure 2e). However, it possessed an obvious increased crystal thickness in comparison with Al-ECNU-7P obtained at 72 h. This indicated that Al-ECNU-7P was a metastable phase formed during the whole crystallization process. The organic CTAB molecules were loosely incorporated between MWW layers because there were no channels perpendicular to the MWW layers that could accommodate or stabilize the long chain organic molecules. Thus, they were readily excluded out of the interlayer spaces, leading to a more stable MCM-22P like precursor. Moreover, the sample obtained at 96 h had a different platelet length in comparison to the pristine ITQ-1 (Figure 2a). This result further verified the multilayer structure of Al-ECNU-7P was not constructed by simply swelling of ITQ-1. The hydrothermal process experienced multisteps of dissolution, assembling and recrystallization, which was different from that recently proposed ADOR process[42-46] and the post-swelling process.[16,21-22]

The TEM images of the products were consistent with the stepwise structural changes that were mentioned above (Figure 3). The initial phase gave a poorly ordered hexagonal mesostructured material (Figure 3a), which transformed to a lamellar intermediate still with a mesostructure but probably containing partially crystallized units in walls (Figure 3b). The TEM images of Al-ECNU-7P confirmed the presence of MWW layers stacking along the *c* direction with large interlayer spacing ranging from 1.6 to 2.4 nm (Figure 3c). The observed interlayer distance between MWW layers was slightly smaller than that determined by PXRD possibly due to a partial removal of CTAB molecules during the sample preparation before HRTEM measurement together with a partial interlayer shrinkage under vacuum conditions during imaging operation. Moreover, it could be determined that over 90 % of MWW layers in Al-ECNU-7P were swelled and pillared by CTAB surfactants from 10 HRTEM images.

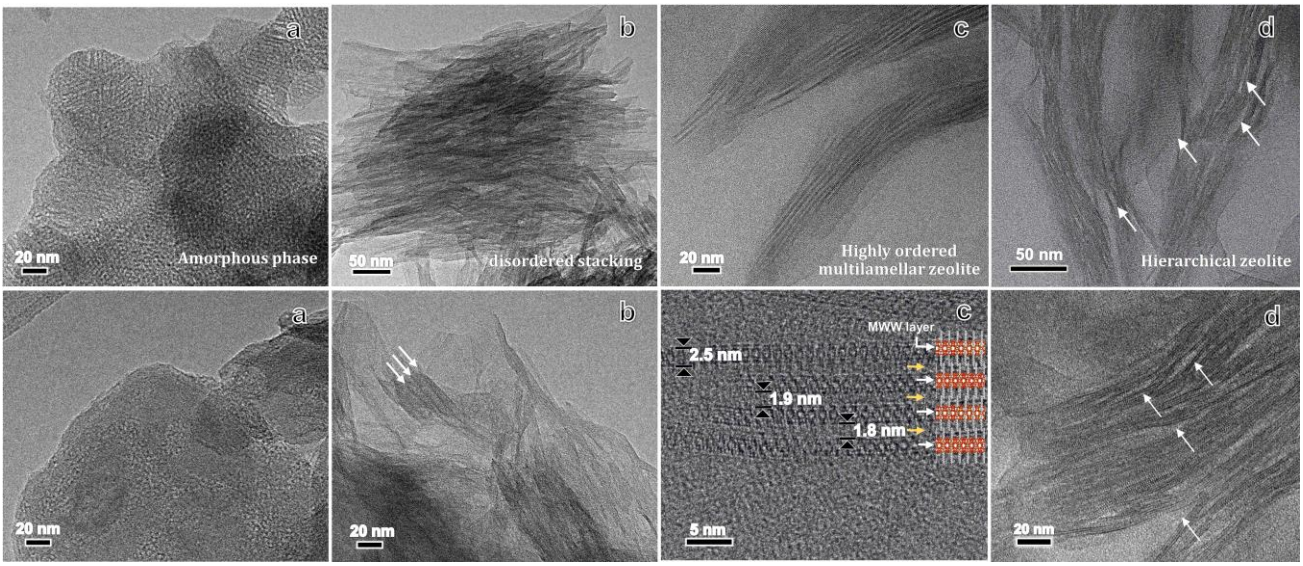

Figure 3. HRTEM images of the samples obtained during the progressive crystallization in Stage II. (a) 423 K, 24 h, (b) 423 K, 48 h, (c) 423 K, 72 h of Al-ECNU-7P (Si/Al = 50), and (d) the calcined form Al-ECNU-7 (Si/Al = 15).

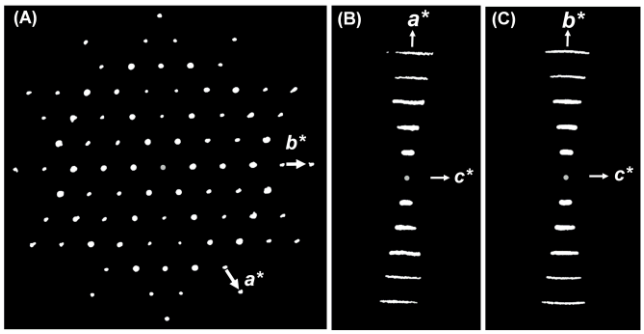

Figure 4. (A) The reconstructed reciprocal lattice from RED data projected along *c**. Selected planes in the reciprocal lattice and corresponding to (B) *hol* and (C) *okl* planes, respectively.

Moreover, the recently developed technique, rotation electron diffraction (RED), allows 3D reciprocal space reconstruction of a crystal based on a series of SAED patterns.[47-48] 300 SAED patterns were collected around an arbitrary axis at 0.2° intervals from a randomly selected Al-ECNU-7P crystal. RED data could provide crystal information of both the layer structure and layers stacking sequence. Strong diffractions were observed from the *c** projection of the reconstructed reciprocal space (Figure 4A), and the unit cell parameters were determined to be a = 13.9 Å, b = 14.0 Å and γ = 118.7°, which were similar as those of traditional 3D MWW zeolite.[36] This indicated that a high structure order of MWW structure was preserved within the layers. Besides, most diffractions in the *hol* and o*kl* planes appeared to be elongated as streaks, indicating a certain degree of structural distortion along *c* direction in Al-ECNU-7P (Figure 4B, 4C and Movie S1), which was likely associated with the somewhat disorder stacking of MWW layers.

Thus, on the basis of the characterizations captured at different synthesis stages, it could be confirmed that the multilamellar MWW zeolite with a large interlayer spacing was hydrothermally synthesized through a dissolution-recrystallization route. The desirable Al-ECNU-7P zeolite could be synthesized by controlling the synthesis condition, especially the crystallization time. The self-assembly of simple surfactant CTAB and the growth of microporous crystalline framework are compatible with each other to generate the multilamellar structure.

Synthesis of ECNU-7P with various Al contents. The syntheses of the swelling-type multilamellar ECNU-7P zeolite were also carried out by varying the synthesis parameters. The following synthetic variables were considered: Si/Al molar ratio (set at 15, 30, 50, 100 and ∞), the molar percentage of ITQ-1 silicate added in starting material (set at 100 %, 75 %, 50 %, 25 % and 0 %), while the OSDA/Si molar ratio was fixed at 0.5. The resulting crystallization field diagram and the optimized crystallization time are summarized in Figure S4. Firstly, when ITQ-1 silicate was used as the sole starting material, the multilamellar MWW zeolites were successfully obtained in the Si/Al ratio range of 15 ~ ∞. The Si/Al ratios of the resultant zeolite products were nearly the same as that of the gel composition. As shown in Figure S5, the low-angle PXRD peak, corresponding to the 001 reflection, decreased in intensity as the Al content in zeolite increased, implying a loss of multilamellar ordering due to the Al incorporation. Besides, increasing the amount of Al source prolonged the optimized crystallization time to 96 h for achieving the well-ordered ECNU-7P in the case of Si/Al ratio = 15 (Figure S4).

When the mixture of ITQ-1 silicate (75 %) and fumed silica (25 %) was adopted as the starting material, ECNU-7P could be prepared with the incorporated Al amount corresponding to the lowest Si/Al ratio of 30. At higher Al content such as Si/Al = 15, the mixture of amorphous silica phase and disordered MWW zeolite nanosheets or conventional MWW zeolite was obtained. When the molar ratio of fumed silica in the starting material increased to 50 %, the synthesis for ECNU-7P could be performed in the Si/Al range of 50 ~ ∞. When the percentage of the fumed silica further increased to 75 %, the synthesis of such swollen materials could only be prepared with the Al content up to Si/Al = 100. Thus the addition of Al source obviously retarded the crystallization process. Notably, the choice of the starting material and the amount of Al introduced were closely relevant with each other, and both of them had a great influence on the formation of the multilamellar MWW zeolite. The variation of these conditions caused some differences in the multilamellar ordering and the optimal time required for hydrothermal reaction. Using ITQ-1 silicate as the sole silica source yield the best structural order within the shortest synthesis time. Decreasing the relative amount of ITQ-1 silicate in the starting silica source would lead to the fully crystallized multilamellar ECNU-7P zeolites with only limited amounts of Al incorporated. On the other hand, it is interesting to explore whether the swelling-type multilamellar MWW structure could be prepared with fumed silica as the sole starting material. No matter whether the Al source was added or not, only amorphous phases were obtained even when the crystallization was prolonged to 168 h in Stage II, as no structural orders due to crystalline microporous framework were detected in high-angle PXRD patterns (Figure S6).

Thus, a high content of ITQ-1 in starting material favored the incorporation of Al into the well-ordered multilamellar MWW zeolite. In syntheses of various zeolites, the seed-assisted technique had been widely applied to shorten the crystallization time or to improve the crystalline quality of the products.[49-52] The existence of specific building units in the gel B would act as seeds helpful for the formation of desirable zeolite structure in the second synthesis stage. The coexistence of these specific silica fragments with zeolitic building units together with suitable OSDA is critical to direct the formation of MWW layers. Thus, the synthesis process must be controlled very delicately using both the thermodynamic and kinetic driving forces.

Investigation into guest-host interaction in multilamellar MWW zeolites. Based on the results from various characterizations, the MWW monolayers in ECNU-7P presumed to be supported by the organic CTAB layers. However, little has been known about the guest-host interaction between the inorganic zeolite layers and organic surfactant. Solid-state NMR spectroscopy is a robust technique to investigate the interaction between inorganic framework and organic surfactant moieties,[53-55] and could provide molecular-level insights into how the self-assembly and crystalline frameworks develop and the role of CTAB surfactant during structure evolution. In this study, the Al source was excluded for simplicity, and the pure silica ITQ-1 was employed as the sole inorganic source in synthesis. The PXRD pattern indicated

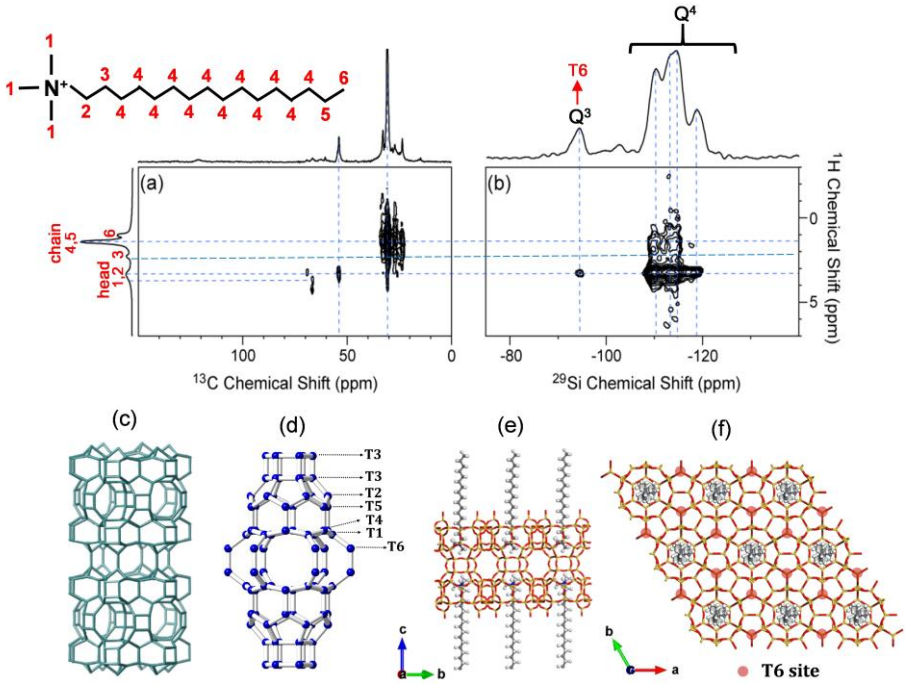

Figure 5. (a) ^{1}H-^{13}C and (b) ^{1}H–^{29}Si HETCOR NMR spectra of Si-ECNU-7P. 1D ^{13}C CP/MAS, ^{29}Si CP/MAS and ^{1}H MAS spectra are shown along the axes. The CP contact time was set to be 0.3 and 4 ms, respectively to acquire ^{1}H-^{13}C and ^{1}H–^{29}Si HETCOR NMR spectra. Skeletal drawings of (c) the framework of 3D MWW structure, (d) the MWW supercage with labeled T atoms and the structure of ECNU-7P viewed along (e) *a* axis and (f) *c* axis.

the resulting Si-ECNU-7P possessed the multilamellar structure with organic CTAB pillars between neighboring MWW layers (Figure S5a). TG analysis indicated that the weight percentage of organic species in Si-ECNU-7P was about 38.2 % (Figure S7). The spatial proximity between zeolite framework and CTAB surfactant could be established with ^{1}H-^{29}Si HETCOR experiment. ^{1}H MAS NMR provided direct information about the surfactant species in zeolites. The ^{1}H NMR chemical shifts were unambiguously assigned according to the ^{1}H-^{13}C HETCOR spectra (Figure 5a), in which only short range correlation could be discerned with a short contact time of 0.3 ms. As shown in Figure 5a, there were two main peaks at *ca.* 1.4 and 3.2 ppm in ^{1}H dimension, which were attributed to the segment methylene (CH_2) group and methyl (CH_3) species directly connected to the ammonium groups of CTAB, respectively. It should be noteworthy that the ^{13}C NMR signals arising from IM^+OH^- were too weak to be well distinguished, probably due to its low concentration.

The 2D ^{1}H-^{29}Si HETCOR NMR spectrum (Figure 5b) revealed the essential role of the CTAB surfactant in supporting the swollen structure of multilamellar MWW zeolites. The ^{29}Si signals in the chemical shift range of –110 ~ -118 ppm, and at -95 ppm were assigned to Q^4 and Q^3 sites in Si-ECNU-7P zeolite, respectively.[28,39] The framework Q^4 sites exhibited the strongest correlation peaks with $-N^+(CH_3)_3$ segment in CTAB, impling the existence of strong intermolecular interactions between the quaternary ammonium head groups of CTAB molecule and the zeolite frameworks, which can further be confirmed from the ^{1}H-^{29}Si HETCOR spectrum obtained with a shorter CP contact time of 1 ms (Figure S8).

As described in the literature,[36,37] a skeletal drawing of 3D MWW structure showing only Si atoms as T sites was shown in Figure 5c. The adjacent MWW layers were joined by Si-O-Si linkages, forming a two-dimensional channel between layers. There were 12 membered-ring (MR) hemicavities on the layer surface and formed a large supercage between layers in 3D MWW zeolite (Figure 5d). However, the hemi-cavities were exposed to the surface of each MWW monolayers in Si-ECNU-7P, as the covalently connection between layers was prevented by organic CTAB layers, only leaving crystallographic T6 site on the layer surface exist freely. Therefore, the Q^3 species in Si-ECNU-7P could only be assigned to the T6 site on the MWW layer surface, while the other T sites were assigned to Q^4 sites with tetrahedral coordination. Thus, it could be deduced that only small parts of CTA^+ surfactants may interact with the free silanols (T6 site). Besides, as the synthesis of ECNU-7P was performed under basic conditions, the head group of the remaining $CTA^+(OH^-)$ may be embedded into the hemicavities of MWW layers through the intermolecular hydrogen-bonding with the bridge oxygen atoms attached to the framework Q^4 sites (Figure 5e and 5f). It is also possible that parts of CTAB surfactants exist freely in the interlayer region in swollen materials.

Besides, the formation of the intermediate amorphous silicate during the crystallization process of Si-ECNU-7P was also evidenced by the solid-state 2D ^{1}H-^{29}Si HETCOR NMR spectrum, which was acquired on the sample after the hydrothermal synthesis for 24 h (Figure S4). The characterization results of the PXRD pattern and SEM image indicated that the amorphous silicate phase might be formed at this crystallization stage (Figure S9), which was similar with that formed during the Al-ECNU-7P (Si/Al = 50) synthesis. Besides, as shown in Figure S10, two broad signals around -100 and -110 ppm were observed in the ^{29}Si NMR spectra, which could be assigned to Q^3 and Q^4 Si species, respectively.

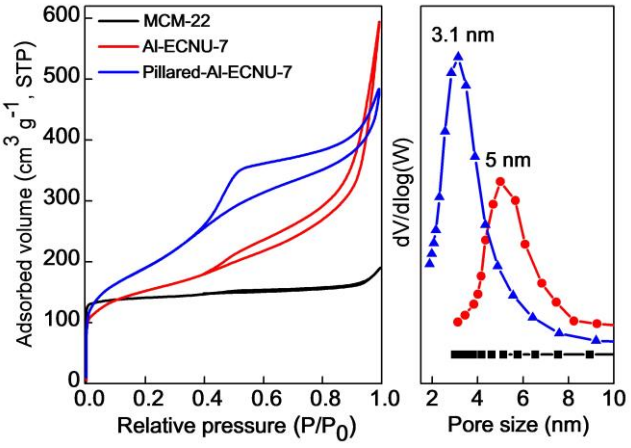

Figure 6. Nitrogen adsorption and desorption isotherms of the calcined conventional MCM-22 (Si/Al = 16), Al-ECNU-7 (Si/Al = 15) and Pillared-Al-ECNU-7 (Si/Al = 22). The mesopore size distribution determined by nitrogen adsorption are showed on the right.

Besides, strong 2D intensity correlations were observed between the Q^3 and Q^4 sites from the amorphous silicate and the ^1H signal at 3.2 ppm from the quaternary ammonium moieties $-N^+(CH_3)$ and $-N^+(CH_2)$ of the CTAB surfactant, indicating that the hydrophilic head group of CTAB molecules directed the formation of mesoporous silica phase at this stage, and then was embedded into the amorphous silica matrix. The interaction in this amorphous sample was greatly different from that in the well-crystallized Si-ECNU-7P, in which the head group of CTAB surfactant only showed strong interaction with Q^4 sites in the 12-MR hemi-cavities (Figure 5). Moreover, this result confirmed the evolution process of ECNU-7P crystallization at the early stage of crystallization, during which the parent ITQ-1 was dissolved to silica segments initially and then self-assembled into weakly ordered mesophase in the presence of CTAB surfactant.

Thus, the NMR analyses on these two samples provided more evidences about the development and evolution process of transient framework structures during the hydrothermal synthesis. The multilamellar Si-ECNU-7P was constructed through the dissolution-recrystallization process, during which the starting source transformed to the intermediate mesoporous amorphous frameworks, and subsequently crystallized into well-ordered assembly of MWW monolayers with large interlayer spacing. The crystallization and the self-assembly were highly coupled, as the simple surfactant CTAB acted as the structure-directing agent for mesophase or pillaring agent for MWW monolayers at different crystallization stages.

Physicochemical properties and catalytic behaviors of hierarchical Al-ECNU-7 zeolite. Considering that at least five different MWW layer stacking modes have been discovered from direct syntheses (MCM-49,[56] MCM-22P,[34] MCM-56,[40] EMM-10P,[39] ECNU-5P[32]), ECNU-7P with swollen structure is a special one, because MWW monolayers are separated by organic CTAB pillars. In addition, the amount of Al incorporated in ECNU-7P could be well controlled in the Si/Al molar range of 15 ~ ∞ by adjusting the Si source ratio of ITQ-1 and amorphous silica. The large interlayer spacing and the high content of Al may provide the opportunity for the construction of the hierarchically structured zeolite catalyst for acid-catalyzed reactions.

The ^{27}Al MAS NMR spectra of both conventional MCM-22 (Si/Al = 16) and Al-ECNU-7 (Si/Al = 15) exhibited a pronounced peak centered at around δ = 55 ppm and a weak peak centered around δ = 0 ppm (Figure S11), that could be attributed to the Al species with tetrahedral and octahedral coordination, respectively.[57] These results demonstrated that most Al atoms in Al-ECNU-7 material were incorporated into the framework. The HRTEM images indicated that the calcined Al-ECNU-7 possessed a hierarchical structure as the MWW sheets were partially condensed and separately arranged (Figure 3d). Apparently, the structural order in the as-synthesized form was lost upon calcination. The mismatching of CTA cation-expanded nanosheets would lead to an incomplete interlayer condensation unlike conventional 3D MWW structure. Then, Al-ECNU-7 was considered to contain a lot of intracrystal mesopores as a result of disordered stacking of MWW layers. In fact, nitrogen adsorption-desorption demonstrated that the calcined Al-ECNU-7 sample showed a combined isotherm of type I and type IV, different from conventional MCM-22 characteristic of typical microporous materials (Figure 6). Al-ECNU-7 had a much higher mesoporosity, and in addition to the micropore of *ca.* 0.55 nm, it showed a very broad mesopore size distribution from 3.8 nm to 8 nm. The total pore volume and external surface area of Al-ECNU-7 were 0.930 $cm^3\ g^{-1}$ and 312 $m^2\ g^{-1}$, respectively (Table S1). On the other hand, the resulting Al-ECNU-7P could be pillared to produce the Pillared-Al-ECNU-7 material, which can be regarded as the analogue to MCM-36.[21-23] As shown in Figure S12, the low angle 001 peak at 2θ = 1.70° was preserved in the pillared sample (in calcined form), indicating the adjacent MWW layers was successfully supported by amorphous silica pillars. Besides, the Pillared-Al-ECNU-7 sample exhibited an increased BET surface area (681 $m^2\ g^{-1}$) and total pore volume (0.663 $cm^3\ g^{-1}$) in comparison with that of conventional MCM-22 (Table S1), while an obvious BJH pore size distribution at 3.1 nm as a result of pillaring was observed (Figure 6). However, the multilamellar Al-ECNU-7P zeolite from hydrothermal synthesis cannot be delaminated simply by ultrasonic treatment in water to yield the exfoliated material like ITQ-2. In contrast, the conventional MCM-22 sample had relatively low total pore volume and external surface area. Therefore, Al-ECNU-7 was a hierarchical MWW material with a high delamination degree,

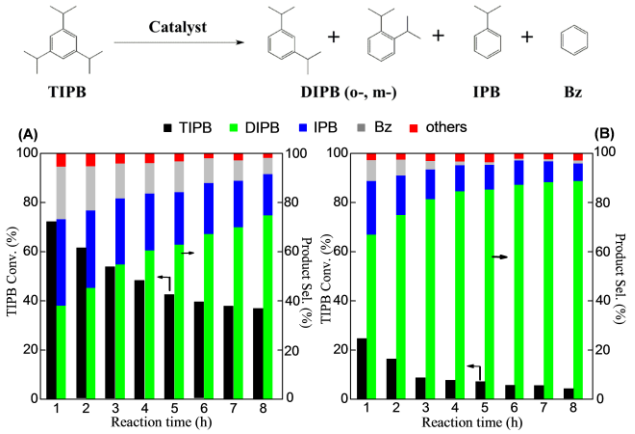

Figure 7. Results of catalytic cracking TIPB over (A) Al-ECNU-7 (Si/Al = 15) and (b) MCM-22 (Si/Al = 16) catalysts. Reaction conditions: cat., 0.2 g; feed rate, 1.7 mL h^{-1}; N_2, 30 mL min^{-1}; temp., 573 K.

Table 1. Catalytic reaction results of the acylation of anisole with anhydride over different catalysts. [a]

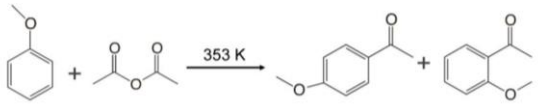

Catalyst	Si/Al [b]	SA [c] ($m^2 g^{-1}$)	ESA [c] ($m^2 g^{-1}$)	SA/ESA	Yield (%)
Al-ECNU-7	31	512	331	1.55	37.1
Pillared-Al-ECNU-7	47	706	605	1.17	48.7
MCM-22	28	452	86	5.26	17.3
MCM-56	32	454	150	3.03	23.3
ZSM-5	31	330	24	13.8	7.8
Beta	29	521	45	11.6	13.4

[a] Reaction condition: cat., 0.1 g; anisole, 5.23 g; acetic anhydride, 5 mmol; temp., 353 K; time, 1 h. [b] Determined by ICP analysis. [c] SA: total surface area, ESA: external surface area.

which would favor the diffusion for bulky molecules in catalytic reactions.

Firstly, the cracking of 1,3,5-triisopropylbenzene (TIPB) was used as a model reaction to assess the catalytic activity of Al-ECNU-7, because its larger external surface may make the active sites more accessible to the substrate, thus would favor the conversion of large molecules. The cracking of TIPB was a successive reaction with the main products as diisopropylbenzene (DIPB) isomers, isopropylbenzene (IPB) and benzene (BZ). Figure 7 showed the changes of TIPB conversion and product selectivities with time-on-stream (TOS). The hierarchical Al-ECNU-7 catalyst exhibited a three times higher TIPB conversion than conventional MCM-22. Although the TIPB conversion decreased with the reaction time for both catalysts, but Al-ECNU-7 exhibited a much slower deactivation rate than MCM-22. On the other hand, the product distribution provided information concerning the extent of cracking degree. Although the selectivity of BZ and IPB decreased with the reaction time, but the selectivity for the deep cracking products over Al-ECNU-7 was also much higher than that of MCM-22 when compared at the same TOS. These results indicated that Al-ECNU-7 showed a better cracking ability than the conventional MCM-22.

In the Friedel-Crafts acylation of anisole with acetic anhydride, the *p*-methoxyacetophenone (*p*-MAP) was the main product with the selectivity over 98 %, which may due to the electronic effect of anisole, the intramolecular steric constraint of *o*-MAP and the electrophilic substitution character of the reaction.[58,59] The comparison was made among the solid-acid catalysts with different zeolite structures. As shown in Table 1, the Al-ECNU-7 and Pillared-Al-ECNU-7 catalysts with hierarchical MWW structure exhibited superior catalytic behaviors, giving rise to 37.1 % and 48.7 % *p*-MAP yield, respectively. In contrast, the conventional MCM-22 and the delaminated MCM-56 with comparable Al loadings only gave 17.3 % and 23.3 % *p*-MAP yield, respectively. As for the bulk H-Al-Beta and H-Al-ZSM-5, lower MAP yields were achieved because of their hydrophilic framework or lacking of mesopores. Notably, the superiority of Al-ECNU-7 and Pillared-Al-ECNU-7 is proportional to its enlarged external surface area and more exposed acid site therein.

CONCLUSIONS

In summary, a swelling-type multilamellar ECNU-7P with alternative stacking of MWW nanosheets and organic CTAB layers was successfully prepared through a dissolution-recrystallization route. It is the first time that the simple surfactant CTAB and layered zeolite precursor could act in a synergetic manner during the self-assembly process. It offers an alternative, attractive pathway to the current post-synthetic approaches or hydrothermal syntheses of MWW nanosheets with designed surfactants. The calcined Al-ECNU-7 turned into a hierarchical zeolite catalyst and exhibited excellent activity, selectivity and stability in the catalytic conversion of bulky molecules. The present approach would be a general methodology and suitable for the direct synthesis of the hierarchical layered zeolites with other topologies by controlling the self-assembly of simple surfactant and zeolite precursor. More significantly, the low cost and commercial availability of simple CTAB surfactant make it more promising than complex bifunctional surfactants for the preparation of industrial heterogeneous catalysts.

ASSOCIATED CONTENT

SUPPORTING INFORMATION

Experimental and characterization information are included. This material is available free of charge via the Internet at http://pubs.acs.org.

AUTHOR INFORMATION

Corresponding Author

*E-mail: pwu@chem.ecnu.edu.cn (P. Wu)

ACKNOWLEDGMENT

We gratefully acknowledge the financial supports from the NSFC of China (21533002 and 21373089), Programs Foundation of MOE of China (2012007613000) and SLAD (B409). Dr. L. Xu acknowledge the financial supports from the China Postdoctoral Science Foundation (2015M580012).

REFERENCES

(1) Corma, A. From Microporous to Mesoporous Molecular Sieve Materials and Their Use in Catalysis. *Chem. Rev.* **1997**, *97*, 2373-2420.
(2) Davis, M. E. Ordered Porous Materials for Emerging Applications. *Nature* **2002**, *417*, 813-821.
(3) Čejka, J.; Mintova, S. Perspectives of Micro/Mesoporous Composites in Catalysis. *Catal. Rev.* **2007**, *49*, 457-509.
(4) Perez-Ramirez, J.; Christensen, C. H.; Egeblad, K.; Christensen, C. H.; Groen, J. C. Hierarchical Zeolites: Enhanced Utilisation of Microporous Crystals in Catalysis by Advances in Materials Design. *Chem. Soc. Rev.* **2008**, *37*, 2530-2542.
(5) Chen, L.; Li, X.; Rooke, J. C.; Zhang, Y.; Yang, X.; Tang, Y.; Xiao, F.; Su, B. Hierarchically Structured Zeolites: Synthesis, Mass Transport Properties and Applications. *J. Mater. Chem.* **2012**, *22*, 17381-17403.
(6) Choi, M.; Cho, H. S.; Srivastava, R.; Venkatesan, C.; Choi, D.; Ryoo, R. Amphiphilic Organosilane-Directed Synthesis of Crystalline Zeolite with Tunable Mesoporosity. *Nat. Mater.* **2006**, *5*, 718-723.
(7) Fan, W.; Snyder, M. A.; Kumar, S.; Lee, P. S.; Yoo, W. C.; McCormick, A. V.; Penn, R. L.; Stein, A.; Tsapatsis, M. Hierarchical Nanofabrication of Microporous Crystals with Ordered Mesoporosity. *Nat. Mater.* **2008**, *7*, 984-991.
(8) Zhang, X. Y.; Liu, D. X.; Xu, D. D.; Asahina, S.; Cychosz, K. A.; Agrawal, K. V.; Al Wahedi, Y.; Bhan, A.; Al Hashima, S.; Terasaki, O.; Thommes, M. Tsapatsis, M. Synthesis of Self-Pillared Zeolite Nanosheets by Repetitive Branching. *Science* **2012**, *336*, 1684-1687.
(9) Zhu, J.; Zhu, Y.; Zhu, L.; Rigutto, M.; Made, A.; Yang, C.; Pan, S.; Wang, L.; Zhu, L.; Jin, Y.; Wu, Q.; Meng, X.; Zhang, D.; Han, Y.; Li, J.; Chu, Y.; Zheng, A.; Qiu, S.; Zheng, X.; Xiao, F. Highly Mesoporous Single-Crystalline Zeolite Beta Synthe-

sized Using a Non-Surfactant Cationic Polymer as a Dual-Function Template. *J. Am. Chem. Soc.* **2014**, *136*, 2503-2510.
(10) Ding, K.; Corma, A.; Macia-Agullo, J. A.; Hu, J. G.; Kramer, S.; Stair, P. C.; Stucky, G. D. Constructing Hierarchical Porous Zeolites via Kinetic Regulation. *J. Am. Chem. Soc.* **2015**, *137*, 11238-11241.
(11) Roth, W. J.; Gil, B.; Makowski, W.; Marszalek, B.; Eliasova, P. Layer Like Porous Materials with Hierarchical Structure. *Chem. Soc. Rev.* **2016**, DOI: 10.1039/ C5CS00508F.
(12) Roth, W. J.; Nachtigall, P.; Morris, R.; Čejka, J. Two-Dimensional Zeolites: Current Status and Perspectives. *Chem. Rev.* **2014**, *114*, 4807-4837.
(13) Roth, W. J.; Čejka, J. Two-Dimensional Zeolites: Dream or Reality? *Catal. Sci. Technol.* **2011**, *1*, 43-53.
(14) Diaz, U.; Corma, A. Layered Zeolitic Materials: an Approach to Designing Versatile Functional Solids. *Dalton Trans.* **2014**, *43*, 10292-10316.
(15) Opanasenko, M. V.; Roth, W. J.; Čejka, J. Two-Dimensional Zeolites in Catalysis: Current Status and Perspectives. *Catal. Sci. Technol.* **2016**, *6*, 2467-2484.
(16) Corma, A.; Fornes, V.; Pergher, S.; Maesen, Th.; Buglass, J. Delaminated Zeolite Precursors as Selective Acidic Catalysts. *Nature* **1998**, *396*, 353-356.
(17) Varoon, K.; Zhang, X.; Elyassi, B.; Brewer, D.; Gettel, M.; Kumar, S.; Lee, J.; Maheshwari, S.; Mittal, A.; Sung, C.; Cococcioni, M.; Francis, L., McCormick, A.; Mkhoyan, A.; Tsapatsis, M. Dispersible Exfoliated Zeolite Nanosheets and Their Application as a Selective Membrane. *Science* **2011**, *334*, 72-75.
(18) Ogion, I.; Nigra, M.; Hwang, S.; Ha, J.; Rea, T.; Zones, S. Katz, A. Delamination of Layered Zeolite Precursors under Mild Conditions: Synthesis of UCB-1 via Fluoride/Chloride Anion-Promoted Exfoliation. *J. Am. Chem. Soc.* **2011**, *133*, 3288-3291.
(19) Gil, B.; Makowski, W.; Marszalek, B.; Roth, W. J.; Kubu, M.; Čejka, J.; Olejniczak, Z. High Acidity Unilamellar Zeolite MCM-56 and Its Pillared and Delaminated Derivatives. *Dalton Trans.* **2014**, *43*, 10501-10511.
(20) Ouyang, X.; Hwang, S.; Runnebaum, R. C.; Xie, D.; Wanglee, Y.; Rea, T.; Zones, S. I.; Katz, A. Single-Step Delamination of a MWW Borosilicate Layered Zeolite Precursor under Mild Conditions without Surfactant and Sonication. *J. Am. Chem. Soc.* **2014**, *136*, 1449-1461.
(21) Roth, W. J.; Kresge, C. T.; Vartuli, J. C.; Leonowicz, M. E.; Fung, A. S.; McCullen, S. B. MCM-36: The First Pillared Molecular Sieve with Zeolite Properties. *Stud. Surf. Sci. Catal.* **1995**, *94*, 301.
(22) Maheshwari, S.; Jordan, E.; Kumar, S.; Bates, F.; Penn, R.; Shantz, D.; Tsapatsis, M. Layer Structure Preservation during Swelling, Pillaring, and Exfoliation of a Zeolite Precursor. *J. Am. Chem. Soc.* **2008**, *130*, 1507-1516.
(23) Roth, W. J.; Čejka, J.; Millini, R.; Montanari, E.; Gil, B.; Kubu, M. Swelling and Interlayer Chemistry of Layered MWW Zeolites MCM-22 and MCM-56 with High Al Content. *Chem. Mater.* **2015**, *27*, 4620-4629.
(24) Choi, M.; Na, K.; Kim, J.; Sakamoto, Y.; Terasaki, O.; Ryoo, R. Stable Single-Unit-Cell Nanosheets of Zeolite MFI as Active and Long-Lived Catalysts. *Nature* **2009**, *461*, 246-250.
(25) Na, K.; Choi, M.; Park, W.; Sakamoto, Y.; Terasaki, O.; Ryoo, R. Pillared MFI Zeolite Nanosheets of a Single-Unit-Cell Thickness. *J. Am. Chem. Soc.* **2010**, *132*, 4169-4177.
(26) Xu, L.; Li, C.; Zhang, K.; Wu, P. Bifunctional Tandem Catalysis on Multilamellar Organic-Inorganic Hybrid Zeolites. *ACS Catal.* **2014**, *4*, 2959-2968.
(27) Xu, D.; Ma, Y.; Jing, Z.; Han, L.; Singh, B.; Feng, J.; Shen, X.; Cao, F.; Oleynikov, P.; Sun, H.; Terasaki, O.; Che, S. π-π Interaction of Aromatic Groups in Amphiphilic Molecules Directing for Single-Crystalline Mesostructures Zeolite Nanosheets. *Nat. Common.* **2014**, 5, 4262.
(28) Xu, D.; Jing, Z.; Cao, F.; Sun, H.; Che, S. Surfactants with Aromatic-Group Tail and Single Quaternary Ammonium Head for Directing Single-Crystalline Mesostructured Zeolite Nanosheets. *Chem. Mater.* **2014**, *26*, 4612-4619.
(29) Singh, B.; Xu, D.; Han, L.; Ding, J.; Wang, Y.; Che, S. Synthesis of Single-Crystalline Mesoporous ZSM-5 with Three-Dimensional Pores via the Self-Assembly of a Designed Triply Branched Cationic Surfactant. *Chem. Mater.* **2014**, *26*, 7183-7188.
(30) Luo, H.; Michaelis, V.; Hodges, S.; Griffin, R.; Roman-Leshkov, Y. One-Pot Synthesis of MWW Zeolite Nanosheets Using a Rationally Designed Organic Structure-Directing Agent. *Chem. Sci.* **2015**, *6*, 6320-6324.
(31) Margarit, V.; Martinez-Armero, M.; Navarro, T.; Martinez, C.; Corma, A. Direct Dual-Template Synthesis of MWW Zeolite Monolayers. *Angew. Chem. Int. Ed.* **2015**, *54*, 13724-13728.
(32) Xu, L. Ji, X.; Jiang, J.; Han, L.; Che, S.; Wu, P. Intergrown Zeolite MWW Polymorphs Prepared by the Rapid Dissolution-Recrystallization Route. *Chem. Mater.* **2015**, *27*, 7852-7860.
(33) Barth, J.; Kornatowski, J. Lercher, J. A. Synthesis of New MCM-36 Derivatives Pillared with Alumina or Magnesia-Alumina. *J. Mater. Chem.* **2002**, *12*, 369-373.
(34) Rubin, M. K.; Chu, P. Composition of Synthetic Porous Crystalline Material, Its Synthesis, and Use. U.S. Patent 4954325, **1990**.
(35) Wang, Y.; Liu, Y.; Wang, L.; Wu, H.; Li, X.; He, M.; Wu, P. Postsynthesis, Characterization, and Catalytic Properties of Aluminosilicates Analogous to MCM-56. *J. Phys. Chem. C* **2009**, *113*, 18753-18760.
(36) Camblor, M.; Corma, A.; Diaz-Cabanas, M.; Baerlocher, C. Synthesis and Structural Characterization of MWW Type Zeolite ITQ-1, the Pure Silica Analog of MCM-22 and SSZ-25. *J. Phys. Chem. B* **1998**, *102*, 44-51.
(37) Leonowicz, M.; Lawton, J.; Lawton, S.; Rubin, M. MCM-22: a Molecular Sieve with Two Independent Multidimensional Channel Systems. *Science* **1994**, *264*, 1910-1913.
(38) Lund, K.; Muroyama, N.; Terasaki, O. Accidental Extinction in Powder XRD Intensity of Porous Crystals: Mesoporous Carbon Crystal CMK-5 and Layered Zeolite-Nanosheets. *Microporous Mesoporous Mater.* **2010**, *128*, 71-77.
(39) Roth, W. J.; Dorset, D.; Kennedy, G. Discovery of new MWW family zeolite EMM-10: Identification of EMM-10P as the Missing MWW Precursor with Disordered Layers. *Microporous Mesoporous Mater.* **2011**, *142*, 168-177.
(40) Fung, A.; Lawton, S.; Roth, W. J. Synthetic Layered MCM-56, Its Synthesis and Use. U.S. Patent 5362697, **1994**.
(41) Archer, R.; Carpenter, J.; Hwang, S.; Burton, A.; Chen, C.; Zones, S.; Davis, M. Physicochemical Properties and Catalytic Behavior of the Molecular Sieve SSZ-70. *Chem. Mater.* **2010**, *22*, 2563-2572.
(42) Roth, W. J.; Shvets, O. V.; Shamzhy, M.; Chlubna, P.; Kubu, M.; Nachtigall, P.; Čejka, J. Postsynthesis Transformation of Three-Dimensional Framework into a Lamellar Zeolite with Modifiable Architecture. *J. Am. Chem. Soc.* **2011**, *133*, 6130-6133.
(43) Roth, W. J.; Nachtigall, P.; Morris, R. E.; Wheatley, P. S.; Seymour, V. R.; Ashbrook, S. E.; Chlubna, P.; Grajciar, L.; Polozij, M.; Zukal, A.; Shvets, O.; Čejka, J. A Family of Zeolites with Controlled Pore Size Prepared Using a Top-Down Method. *Nat. Chem.* **2013**, 5, 628-633.
(44) Mazur, M.; Wheatley, P. S.; Navarro, M.; Roth, W. J.; Polozij, M.; Mayoral, A.; Eliasova, P.; Nachtigall, P.; Čejka, J.; Morris, R. E. Synthesis of 'Unfeasible' Zeolites. *Nat. Chem.* **2016**, *8*, 58-62.
(45) Eliasova, P.; Opanasenko, M.; Wheatley, P. S.; Shamzhy, M.; Mazur, M.; Nachtigall, P.; Roth, W. J.; Morris, R. E.; Čejka, J. The ADOR Mechanism for the Synthesis of New Zeolites. *Chem. Soc. Rev.* **2015**, *44*, 7177-7206.
(46) Morris, R. E.; Čejka, J. Exploiting Chemically Selective Weakness in Solids as A Route to New Porous Materials. *Nat. Chem.* **2015**, *7*, 381-388.
(47) Kolb, U.; Gorelik, T.; Kubel, C.; Otten, M. T.; Hubert, D. Towards Automated Diffraction Tomography: Part I-Data Acquisition. *Ultramicroscopy* **2007**, *107*, 507-513.
(48) Zhang, D. L.; Oleynikov, P.; Hovmoller, S.; Zou, X. D. Collecting 3D Electron Diffraction Data by the Rotation Method. *Z. Kristallogr.* **2010**, *225*, 94-102.
(49) Itabashi, K.; Kamimura, Y.; Iyoki, K.; Shimojima, A.; Okubo, T. A Working Hypothesis for Broadening Framework Types of Zeolites in Seed-Assisted Synthesis without Organic Structure-Directing Agent. *J. Am. Chem. Soc.* **2012**, *134*, 11542-11549.

(50) Xie, B.; Song, J.; Ren, L.; Ji, Y.; Li, J.; Xiao, F. Organotemplate-Free and Fast Route for Synthesizing Beta Zeolite. *Chem. Mater.* **2008**, *20*, 4533-4535.
(51) Majano, G.; Delmotte, L.; Valtchev, V.; Minotova, S. Al-Rich Zeolite Beta by Seeding in the Absence of Organic Template. *Chem. Mater.* **2009**, *21*, 4184-4191.
(52) Yokoi, T.; Yoshioka, M.; Imai, H.; Tatsumi, T. Diversification of RTH-Type Zeolite and Its Catalytic Application. *Angew. Chem. Int. Ed.* **2009**, *48*, 9884-9887.
(53) Na, K.; Jo, C.; Kim, J.; Cho, K.; Jung, J.; Seo, Y.; Messinger, R.; Chmelka, B.; Ryoo, R. Directing Zeolite Structures into Hierarchically Nanoporous Architectures. *Science* **2011**, *333*, 328-332.
(54) Brouwer, D.; Cadars, S.; Eckert, J.; Liu, Z.; Terasaki, O.; Chmelka, B. A General Protocol for Determining the Structures of Molecularly Ordered but Noncrystalline Silicate Frameworks. *J. Am. Chem. Soc.* **2013**, *135*, 5641-5655.
(55) Messinger, R.; Na, K.; Seo, Y.; Ryoo, R.; Chmelka, B. Co-development of Crystalline and Mesoscopic Order in Mesostructured Zeolite Nanosheets. *Angew. Chem. Int. Ed.* **2015**, *54*, 927-931.
(56) Lawton, S. L.; Fung, A. S.; Kennedy, G. J.; Alemany, L. B.; Chang, C. D.; Hatzikos, G. H.; Lissy, D. N.; Rubin, M. K.; Timken, H. K. C.; Steuernagel, S.; Woessner, D. E. Zeolite MCM-49: A Three-Dimensional MCM-22 Analog Synthesized by In Situ Crystallization. *J. Phys. Chem.* **1996**, *100*, 3788-3789.
(57) Moliner, M.; Gonzalez, J.; Portilla, M. T.; Willhammer, T.; Rey, F.; Llopis, F. J.; Zou, X.; Corma, A. A New Aluminosilicate Molecular Sieve with a System of Pores between Those of ZSM-5 and Beta Zeolite. *J. Am. Chem. Soc.* **2011**, *133*, 9497-9505.
(58) Guidotti, M.; Canaff, C.; Coustard, J.; Magnoux, P.; Guisnet, M. Acetylation of Aromatic Compounds over H-BEA Zeolite: the Influence of the Substituents on the Reactivity and on the Catalyst Stability. *J. Catal.* **2005**, *230*, 375-383.
(59) Fan, W.; Wei, S.; Yokoi, T.; Inagaki, S.; Li, J.; Wang, J.; Kondo, J.; Tatsumi, T. Synthesis, Characterization, and Catalytic Properties of H-Al-YNU-1 and H-Al-MWW with Different Si/Al Ratios. *J. Catal.* **2009**, *266*, 268-278.

Self-Assembly of CTAB and Lamellar Zeolite Precursor for the Preparation of Hierarchical MWW Zeolite